Physics Letters B 704 (2011) 347–353

Contents lists available at SciVerse ScienceDirect

Physics Letters B

www.elsevier.com/locate/physletb

Baryon formation and dissociation in dense hadronic and quark matter

Jin-cheng Wang [a,b], Qun Wang [a,c,*], Dirk H. Rischke [b,d]

[a] Interdisciplinary Center for Theoretical Study and Department of Modern Physics, University of Science and Technology of China, Anhui 230026, People's Republic of China
[b] Institute for Theoretical Physics, Johann Wolfgang Goethe University, Max-von-Laue-Str. 1, D-60438 Frankfurt am Main, Germany
[c] Theoretical Physics Center for Science Facilities, Chinese Academy of Sciences, Beijing 100049, People's Republic of China
[d] Frankfurt Institute for Advanced Studies, Ruth-Moufang-Str. 1, D-60438 Frankfurt am Main, Germany

ARTICLE INFO

Article history:
Received 21 March 2011
Received in revised form 6 September 2011
Accepted 12 September 2011
Available online 16 September 2011
Editor: J.-P. Blaizot

ABSTRACT

We study the formation of baryons as composed of quarks and diquarks in hot and dense hadronic matter in a Nambu–Jona-Lasinio (NJL)-type model. We first solve the Dyson–Schwinger equation for the diquark propagator and then use this to solve the Dyson–Schwinger equation for the baryon propagator. We find that stable baryon resonances exist only in the phase of broken chiral symmetry. In the chirally symmetric phase, we do not find a pole in the baryon propagator. In the color-superconducting phase, there is a pole, but it has a large decay width. The diquark does not need to be stable in order to form a stable baryon, a feature typical for so-called Borromean states. Varying the strength of the diquark coupling constant, we also find similarities to the properties of an Efimov state.

A baryon is a color-singlet bound state of three constituent quarks. Since the interaction between two quarks is attractive in the color-antitriplet channel, baryon formation can be regarded as a two-step process: first, two quarks combine to form a diquark with color-antitriplet quantum numbers, and then this diquark combines with another color-triplet quark to form a color-singlet bound state [1–9].

At extremely high baryonic densities and low temperatures quarks form Cooper pairs in the attractive color-antitriplet channel, leading to the phenomenon of color superconductivity [10–13] (for recent reviews, see e.g. Refs. [14,15]). Because of asymptotic freedom, the interaction is weak and, just like in BCS theory, the Cooper pair wave function has a correlation length that exceeds the interparticle distance. However, as the density is lowered, the interaction strength increases and the Cooper pair becomes more and more localized [16,17]. Eventually, Cooper pairs will form tightly bound molecular diquark states [18]. These may pick up another quark with the right color to form a color-singlet baryon. This is what must happen across the deconfinement transition into the hadronic phase. Understanding the nature of the transition between dense hadronic and quark matter is one of the scientific goals of the Compressed Baryonic Matter (CBM) experiment planned at the Facility for Antiproton and Ion Research (FAIR) [19].

In this Letter we investigate the formation and dissociation of baryons in different regions of the phase diagram of strongly interacting matter: the phase of broken chiral symmetry (hadronic phase), the phase of restored chiral symmetry (the quark–gluon plasma) above and below the dissociation boundary for diquarks, and the phase where quark matter is a color superconductor. We use an NJL-type model [20,21] for two quark flavors and employ the following strategy. First, we compute the full propagator for the scalar diquark state via solving a Dyson–Schwinger equation. With the diquark propagator and an additional quark propagator, we then solve a Dyson–Schwinger equation for the baryon propagator.

Our approach bears some similarities to previous studies of diquark and baryon formation [22–26]. These works also considered an NJL-type model, but they solved the full Faddeev equation instead of a (simpler) Dyson–Schwinger equation to obtain baryon states. The difference is that in the Faddeev equation the coupling between quark and diquark is not assumed to be local: a non-static quark can be exchanged between them. Our work is based on the cruder approximation of a local quark–diquark coupling. These works also considered the axial-vector diquark state, not only the scalar one, and thus were able to investigate also excited baryon states. On the other hand, in those works only the zero-temperature case was studied, while we also consider non-zero temperature. Moreover, we do not assume the diquark to be a well-defined quasi-particle in order to solve the Dyson–Schwinger equation (an approximation employed in the aforementioned works in order to solve the Faddeev equation). We shall see that diquarks can also be unstable, but still give rise to stable

* Corresponding author at: Interdisciplinary Center for Theoretical Study and Department of Modern Physics, University of Science and Technology of China, Anhui 230026, People's Republic of China.
E-mail address: qunwang@ustc.edu.cn (Q. Wang).

0370-2693
doi:10.1016/j.physletb.2011.09.037

baryons, a typical feature of a Borromean state also encountered in atomic and nuclear physics. Varying the diquark coupling strength, we also find that our baryon has properties which bear similarities to those of an Efimov state. We use natural units $\hbar = c = k_B = 1$; the metric tensor is $g_{\mu\nu} = \mathrm{diag}(+,-,-,-)$.

The Lagrangian of the two-flavor NJL model with diquark–diquark interactions reads

$$\begin{aligned}\mathcal{L}_{NJL} &= \overline{\psi}\big(i\gamma_\mu\partial^\mu - \hat{m}_0 + \hat{\mu}\gamma_0\big)\psi \\ &\quad + G_S\big[(\overline{\psi}\psi)^2 + (\overline{\psi}i\gamma_5\boldsymbol{\tau}\psi)^2\big] \\ &\quad + G_D[\overline{\psi}i\gamma_5\tau_2 J_a\psi_C][\overline{\psi}_C i\gamma_5\tau_2 J_a\psi]. \end{aligned} \tag{1}$$

Here, we have suppressed the color indices in the fundamental representation, $a = 1,2,3$, and the flavor indices, $\alpha = u,d$, in the quark spinors $\psi \equiv \psi_{a\alpha}$. The bare mass matrix is $\hat{m}_0 = \mathrm{diag}(m_u^{(0)}, m_d^{(0)})$ and the chemical potential matrix is $\hat{\mu} = \mathrm{diag}(\mu_u, \mu_d)$, τ_s $(s = 1,2,3)$ are the Pauli matrices in flavor space, $(J_a)_{bc} = -i\epsilon_{abc}$ are the antisymmetric color matrices, G_S and G_D are coupling constants for quark–antiquark and quark–quark interactions, respectively. In principle, G_D can be related to G_S via a Fierz transformation, but we choose to keep it as a free parameter, allowing to explore a wider range of potentially interesting phenomena within our effective model for the strong interaction.

In the following, we neglect the contribution from the isovector quark–antiquark channel, $\overline{\psi}i\gamma_5\boldsymbol{\tau}\psi = 0$. We also decompose the scalar quark current in terms of a condensate part and a fluctuation, $\bar{\psi}_\alpha\psi_\alpha = \sigma_\alpha + \delta_\alpha$, where $\sigma_\alpha = \langle\overline{\psi}_\alpha\psi_\alpha\rangle$ is the chiral condensate, and we work in the mean-field approximation, i.e., we neglect terms of order $O(\delta_\alpha^2)$. Similarly, we decompose the diquark current as $\overline{\psi}i\gamma_5\tau_2 J_a\psi_C = (\Delta_a + \delta_a)/(2G_D)$ and drop the quadratic term in δ_a, where the diquark condensate is $\Delta_a = 2G_D\langle\overline{\psi}i\gamma_5\tau_2 J_a\psi_C\rangle$. The diquark condensate fluctuation can be introduced by the replacement $\Delta_a \to \Delta_a + \varphi_a$ and keeping quadratic terms in the fluctuation φ_a. The above operation is equivalent to performing the Hubbard–Stratonovich transformation in the diquark sector. The Lagrangian (1) now becomes

$$\begin{aligned}\mathcal{L}_{NJL} &\approx -\frac{1}{2}\overline{\Psi}S^{-1}\Psi - \frac{1}{4G_D}\sum_a|\Delta_a|^2 - G_S(\sigma_u+\sigma_d)^2 \\ &\quad - \frac{1}{8G_D}\big(\varphi_{aR}^2 + \varphi_{aI}^2\big) + \frac{1}{2}\overline{\Psi}\varphi_{ai}\widehat{\Gamma}_{ai}\Psi. \end{aligned} \tag{2}$$

Here $\Psi = (\psi, \psi_C)^T$ and $\overline{\Psi} = (\overline{\psi}, \overline{\psi}_C)$ are quark spinors in the Nambu–Gorkov (NG) basis. The charge-conjugate spinors are defined by $\psi_C = C\overline{\psi}^T$ and $\overline{\psi}_C = \psi^T C$ with $C = i\gamma^2\gamma^0$. The complex diquark fluctuation φ_a has been decomposed in terms of its real and imaginary parts, $\varphi_a = (\varphi_{aR} + i\varphi_{aI})/\sqrt{2}$, with color indices $a = 1,2,3$. The inverse fermion propagator S^{-1} in the NG basis is given by

$$S^{-1}(P) = -\begin{pmatrix} P_\mu\gamma^\mu + \hat{\mu}\gamma^0 - \hat{m} & i\gamma_5\tau_2 J_a\Delta_a^\dagger \\ i\gamma_5\tau_2 J_a\Delta_a & P_\mu\gamma^\mu - \hat{\mu}\gamma^0 - \hat{m}\end{pmatrix}, \tag{3}$$

where $\hat{m} = \mathrm{diag}(m_u, m_d)$ is the quark mass matrix with corrections from chiral condensates, $m_i = m_i^{(0)} - 2G_S(\sigma_u + \sigma_d)$ with $i = u,d$. The quark–quark–diquark vertices $\widehat{\Gamma}_{ai}$ are given by $\widehat{\Gamma}_{aR} = \frac{i}{\sqrt{2}}\gamma_5\tau_2 J_a\tau_1^{NG}$, $\widehat{\Gamma}_{aI} = \frac{i}{\sqrt{2}}\gamma_5\tau_2 J_a\tau_2^{NG}$, where τ_s^{NG} $(s = 1,2,3)$ are Pauli matrices in NG space. In the following, without loss of generality we choose the diquark condensate to be $\Delta_a = \delta_{a3}\Delta_3$. Note that we only consider the scalar channel for the diquark condensate, as we are only interested in the lowest baryon state, not the higher-lying excited ones. Including the axial-vector channel is straightforward, but will not modify our results qualitatively. Finally, we remark that the tadpole term $\varphi_a\Delta_a^* + \varphi_a^*\Delta_a$, which in principle also appears in Eq. (2), is cancelled by the term $\varphi_a\overline{\psi}_C i\gamma_5\tau_2 J_a\psi + \varphi_a^*\overline{\psi}i\gamma_5\tau_2 J_a\psi_C$ at the one-loop level, where $\overline{\psi}_C\psi + \overline{\psi}\psi_C$ contracts and forms a quark loop in the NG basis. The cancellation condition is just the gap equation for Δ.

We now add the baryon field to our Lagrangian. We assume the baryon to be generated by an interaction term between two quark and two diquark fields,

$$\begin{aligned}\mathcal{L}_B &= G_B\varphi_a^\dagger\bar{\psi}_a\psi_b\varphi_b \\ &\simeq -\frac{1}{2G_B}\bar{\mathbf{B}}\mathbf{B} + \frac{1}{2}\bar{\mathbf{B}}\widehat{\Gamma}_{Bi}\Psi_a\varphi_{ai} + \frac{1}{2}\varphi_{ai}\overline{\Psi}_a\widehat{\Gamma}_{Bi}^*\mathbf{B}. \end{aligned} \tag{4}$$

Here, we decomposed $\psi_a\varphi_a = \langle\psi_a\varphi_a\rangle + \beta_a$, defined the baryonic field as $B = G_B\langle\psi_a\varphi_a\rangle$, and neglected terms of order $O(\beta_a^2)$. The baryonic fields in the NG basis are then denoted by $\mathbf{B} = (B, B_c)^T$ and $\bar{\mathbf{B}} = (\bar{B}, \bar{B}_c)$. The baryon–quark–diquark vertices are $\widehat{\Gamma}_{BR} = \frac{1}{\sqrt{2}}1_{NG}$ and $\widehat{\Gamma}_{BI} = i\frac{1}{\sqrt{2}}\tau_3^{NG}$, respectively. The sum of the Lagrangians (2) and (4) is the starting point for our further treatment. In the following, for the sake of simplicity we assume exact isospin symmetry and we work in the chiral limit, i.e., $\sigma_u = \sigma_d \equiv \sigma$, thus $m_u = m_d = m_q$, $\mu_u = \mu_d = \mu_q$, and $m_u^{(0)} = m_d^{(0)} \equiv 0$.

We now derive the full diquark propagator via the Dyson–Schwinger equation,

$$D_{i,a}^{-1}(p_0,\mathbf{p}) = -\frac{1}{4G_D} - \Pi_{i,a}(p_0,\mathbf{p}), \tag{5}$$

where $p_0 = i2\pi nT$ are the bosonic Matsubara frequencies $(n = 0, \pm1, \pm2, \ldots)$, $i,j = R,I$, and $a,b = 1,2,3$ are fundamental colors. The full propagator $D_{i,a}$ and the self-energy $\Pi_{i,a}$ only carry one index $i = R,I$ and one color index a, because they are diagonal in the space of R,I and in color space. The self-energy has the property $\Pi_{R/I,a} = \frac{1}{2}(\Pi_0^a \pm \Pi_1^a)$, where Π_0^a and Π_1^a depend on the diagonal and the off-diagonal parts of the quark propagator, respectively, and $\Pi_1^a = \delta_{a3}\Pi_1^3$. The expressions for $\Pi_0^a(p_0,\mathbf{p})$ and $\Pi_1^a(p_0,\mathbf{p})$ are

$$\begin{aligned}\Pi_0^{1,2} &= 2\int\frac{d^3k}{(2\pi)^3}c_{k,p+k} \\ &\quad\times\Bigg[\frac{e_1'\epsilon_k^{e'} + \xi_k^{e'}}{2e_1'\epsilon_k^{e'}}\frac{1 - f(e_1'\epsilon_k^{e'}) - f(\xi_{p+k}^e)}{p_0 - e_1'\epsilon_k^{e'} - \xi_{p+k}^e} \\ &\quad + \frac{e_1\epsilon_{p+k}^e + \xi_{p+k}^e}{2e_1\epsilon_{p+k}^e}\frac{1 - f(\xi_k^{e'}) - f(e_1\epsilon_{p+k}^e)}{p_0 - \xi_k^{e'} - e_1\epsilon_{p+k}^e}\Bigg], \\ \Pi_0^3 &= 4\int\frac{d^3k}{(2\pi)^3}\frac{e_1'\epsilon_k^{e'} + \xi_k^{e'}}{2e_1'\epsilon_k^{e'}}\frac{e_1\epsilon_{p+k}^e + \xi_{p+k}^e}{2e_1\epsilon_{p+k}^e} \\ &\quad\times\frac{1 - f(e_1'\epsilon_k^{e'}) - f(e_1\epsilon_{p+k}^e)}{p_0 - e_1'\epsilon_k^{e'} - e_1\epsilon_{p+k}^e}c_{k,p+k}, \\ \Pi_1^{1,2} &= 0, \\ \Pi_1^3 &= -\int\frac{d^3k}{(2\pi)^3}\frac{\Delta_3^2}{e_1e_1'\epsilon_k^e\epsilon_{p+k}^{e'}} \\ &\quad\times\frac{1 - f(e_1\epsilon_k^e) - f(e_1'\epsilon_{p+k}^{e'})}{p_0 - e_1\epsilon_k^e - e_1'\epsilon_{p+k}^{e'}}c_{k,p+k}, \end{aligned} \tag{6}$$

where summations over $e,e',e_1,e_1' = \pm1$ are implied, $f(x) = 1/(e^{x/T}+1)$ is the Fermi–Dirac distribution, $E_k = \sqrt{k^2 + m_q^2}$, $\xi_k^e = eE_k - \mu$, $\epsilon_k^e = \sqrt{(\xi_k^e)^2 + \Delta^2}$, and $c_{k,p+k} = 1 + ee'\frac{\mathbf{k}\cdot(\mathbf{p}+\mathbf{k}) + m_q^2}{E_kE_{p+k}}$.

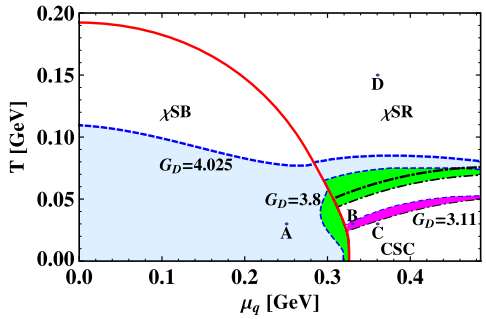

Fig. 1. The phase diagram obtained within our model. For explanations see text. (For interpretation of the references to color in this figure, the reader is referred to the web version of this Letter.)

Some simple properties of $D_{i,a}^{-1}$ are: (1) $D_{R,3}^{-1} \neq D_{I,3}^{-1}$ when $\Delta_3 \neq 0$; (2) $D_{i,1}^{-1} = D_{j,2}^{-1}$ for any $i, j = R, I$; (3) $D_{i,1}^{-1} = D_{i,2}^{-1} = D_{i,3}^{-1} = D^{-1}$ when $\Delta_3 = 0$ for any $i = R, I$. We also have $\Pi_1^a = 0$ when $\Delta_a = 0$. The spectral density for diquarks is then given by

$$\rho_{i,a}(\omega, \mathbf{p}) = \frac{1}{\pi} \frac{\operatorname{Im} D_{i,a}^{-1}(\omega + i\eta, \mathbf{p})}{[\operatorname{Re} D_{i,a}^{-1}(\omega + i\eta, \mathbf{p})]^2 + [\operatorname{Im} D_{i,a}^{-1}(\omega + i\eta, \mathbf{p})]^2}, \tag{7}$$

where we analytically continued $p_0 \to \omega + i\eta$ with real ω and η a small positive number. We have similar properties for the spectral densities as for $D_{i,a}^{-1}$. With the spectral density, we can obtain the full propagator via the dispersion relation

$$D_{i,a}(p_0, \mathbf{p}) = \int_{-\infty}^{\infty} d\omega \, \frac{\rho_{i,a}(\omega, \mathbf{p})}{\omega - p_0}. \tag{8}$$

From the Lagrangian (4) the 11-component in NG space of the inverse baryon propagator is $S_B^{-1} = -1/(2G_B) - \Sigma$, where

$$\Sigma(P) = -\frac{1}{4} \sum_a \int_K S_{11}^a(P - K)\big[D_{R,a}(K) + D_{I,a}(K)\big] \tag{9}$$

is the 11-component of the baryon self-energy. The quark propagator in NG space, S_{11}^a, is diagonal in color space. In the presence of a non-vanishing diquark condensate, $S_{11}^1 = S_{11}^2 \neq S_{11}^3$. If the diquark condensate vanishes, $S_{11}^1 = S_{11}^2 = S_{11}^3$ and $D_{R,a} = D_{I,b}$ for any a, b. In order to evaluate Σ, we insert Eq. (8) into Eq. (9). Since we are interested in baryons at rest, we shall take the $\mathbf{p} = \mathbf{0}$ limit of the positive energy component of S_B^{-1}, $S_{B,+}^{-1}(p_0, \mathbf{p} = \mathbf{0}) = \frac{1}{2} \operatorname{Tr}[S_B^{-1} \Lambda_{\mathbf{p}=\mathbf{0}}^{+} \gamma^0]$, where $\Lambda_{\mathbf{p}}^s$ is the energy projector $\Lambda_{\mathbf{p}}^s = \frac{1}{2}[1 + s(\gamma_0 \boldsymbol{\gamma} \cdot \mathbf{p} + \gamma_0 M_B)/E_p]$, with $E_p = \sqrt{p^2 + M_B^2}$ and $s = \pm 1$. In the homogeneous limit, $\mathbf{p} = \mathbf{0}$, the energy projector assumes a simple form, $\Lambda_{\mathbf{p}=\mathbf{0}}^s = \frac{1}{2}(1 + s\gamma_0)$, which is independent of M_B. Then, we obtain the spectral density as

$$\rho_B(\omega, \mathbf{p}) = \frac{1}{\pi} \frac{\operatorname{Im} S_{B,+}^{-1}(\omega + i\eta, \mathbf{0})}{[\operatorname{Re} S_{B,+}^{-1}(\omega + i\eta, \mathbf{0})]^2 + [\operatorname{Im} S_{B,+}^{-1}(\omega + i\eta, \mathbf{0})]^2}, \tag{10}$$

where we have again analytically continued $p_0 \to \omega + i\eta$.

In our calculations for Figs. 1–6, we choose the following parameters: $G_S = 5.1$ GeV^{-2}, $\Lambda = 0.65$ GeV (momentum cutoff). For Figs. 1 and 6, we vary G_D, in order to investigate the effect of the diquark coupling constant on the boundaries of the diquark dissociation and the color-superconducting (CSC) phase and on the baryon formation. For Figs. 2–5, we set $G_D = 3.11$ GeV^{-2}. This value is in the weak-coupling region, so the diquark is unstable in the phase of broken chiral symmetry. Nevertheless, we shall show that a quark and an unstable diquark can form a stable baryon in this phase. For Figs. 4–6, we choose $G_B = 10.04$ GeV^{-1}. The baryon coupling constant G_B is actually the static approximation for an intermediate quark propagator in the Faddeev equation. This approximation allows us to investigate baryon properties also at non-zero temperature and density. We fix G_B to obtain a baryon mass of 940 MeV in the vacuum.

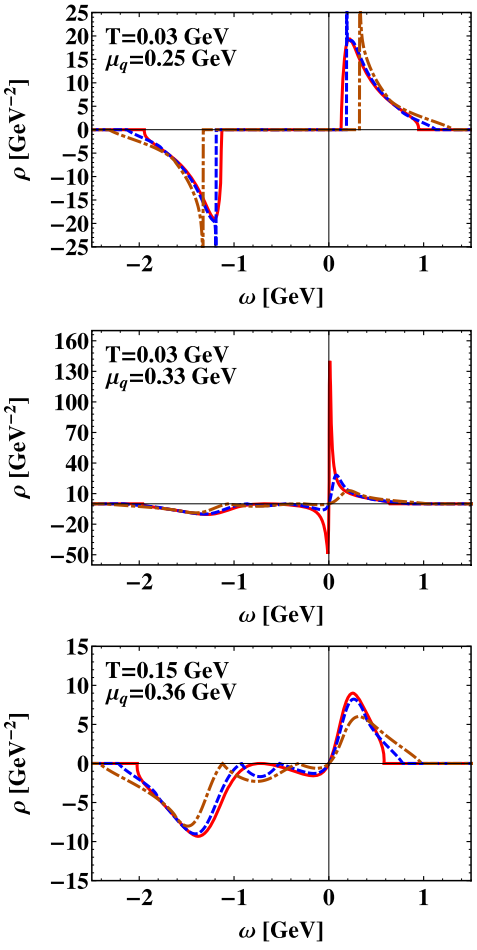

Fig. 2. Diquark spectral densities for different values of T and μ_q. The upper panel corresponds to the point A in the phase diagram with $(T, \mu_q) = (0.03, 0.25)$. The middle panel corresponds to the point B in the phase diagram with $(T, \mu_q) = (0.03, 0.33)$. The lower panel is in the chiral symmetric phase, corresponding to the point D in the phase diagram with $(T, \mu_q) = (0.15, 0.36)$. For all panels we have $\rho \equiv \rho_R = \rho_I$. The red solid lines are for $p = 0$, the blue dashed and brown dash-dotted lines are for $p = 0.2$ and $p = 0.4$, respectively. All units in GeV. (For interpretation of the references to color in this figure, the reader is referred to the web version of this Letter.)

In the phase diagram of Fig. 1, we choose four sets of values for temperature and quark chemical potential, $(T, \mu_q) = (0.03, 0.25), (0.03, 0.33), (0.03, 0.36)$, and $(0.15, 0.36)$, all in GeVs. They correspond to points A, B, C, and D. The red solid line separates the regions (indicated by χSB/χSR) where chiral symmetry is broken/restored; CSC denotes the color-superconducting phase. The blue dashed lines show the diquark dissociation boundaries for three values of the diquark coupling constant, $G_D = 3.11, 3.8, 4.025$ (in units of GeV^{-2}). Below a diquark dissociation line, the equation $\operatorname{Re} D^{-1}(\omega, \mathbf{p} = \mathbf{0}) = 0$ has a real solution ω, the so-called diquark pole. The corresponding regions in Fig. 1 are

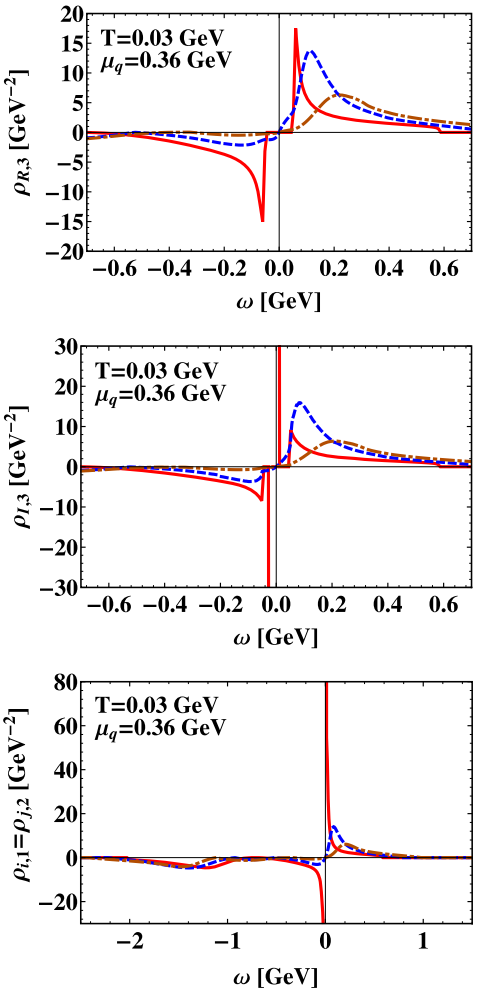

Fig. 3. Diquark spectral densities for different values of T and μ_q. The upper, middle and lower panels are $\rho_{R,3}$, $\rho_{I,3}$ and $\rho_{I/R,1/2}$ in the CSC phase, respectively, corresponding to the point C in the phase diagram with $(T, \mu_q) = (0.03, 0.36)$. The red solid lines are for $p = 0$, the blue dashed and brown dash-dotted lines are for $p = 0.2$ and $p = 0.4$, respectively. All units in GeV. (For interpretation of the references to color in this figure, the reader is referred to the web version of this Letter.)

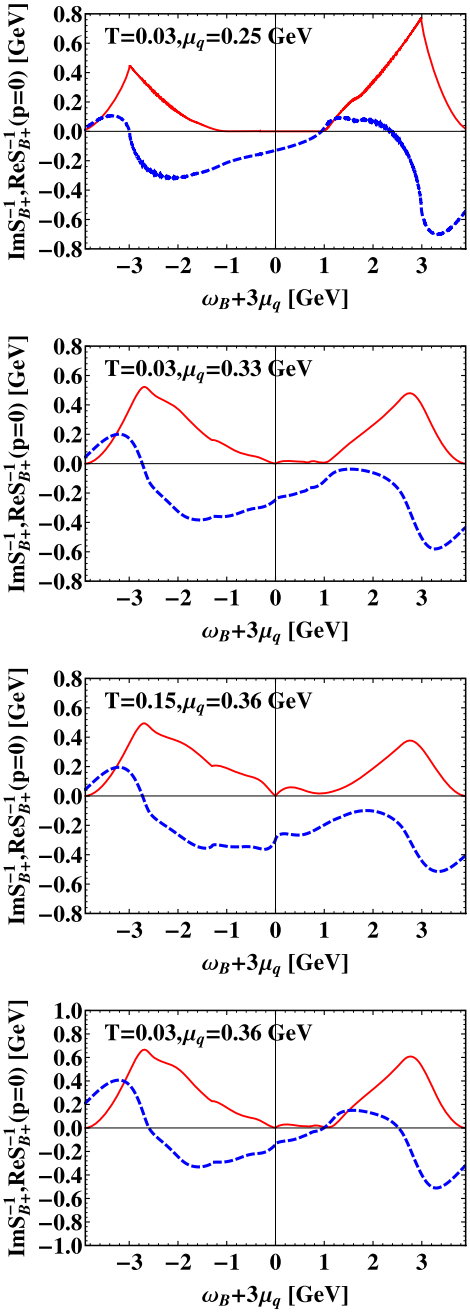

Fig. 4. The real (blue dashed) and imaginary (red solid) parts of the inverse propagators for baryons as functions of energy ω at different T and μ_q. From top to bottom, the first panel: $T = 0.03$ and $\mu_q = 0.25$ (point A). The second panel: $T = 0.03$ and $\mu_q = 0.33$ (point B). The third panel: $T = 0.15$ and $\mu_q = 0.36$ (point D). The fourth panel: $T = 0.03$ and $\mu_q = 0.36$ (point C). All units in GeV. (For interpretation of the references to color in this figure, the reader is referred to the web version of this Letter.)

filled with light blue, green, and magenta color, respectively. These poles also exist in the CSC phases, however, for the sake of clarity we choose not to color the respective regions. The CSC phases are bounded by the red solid line from the left and by the dash-dotted lines from above (from bottom to top for $G_D = 3.11, 3.8, 4.025$, respectively). Note that the diquark coupling constants we have chosen here are in the weak-coupling or BCS regime. As we increase G_D, Bose–Einstein condensation of diquarks could take place in the region below the dissociation lines, provided the bare quark mass is non-zero [18,27–32]. Note that in Ref. [18], a vanishing decay width was imposed as an additional criterion for the location of the dissociation boundary.

The numerical results for the spectral densities are presented in Figs. 2–3. The upper panel of Fig. 2 shows the diquark spectral densities in the phase of broken chiral symmetry (point A of Fig. 1). In the homogeneous limit ($\mathbf{p} = \mathbf{0}$, red solid line), no diquark poles exist (since $G_D = 3.11$ GeV^{-2} is too small), and the curves are smooth. The middle panel shows the diquark spectral densities in the phase of restored chiral symmetry, below the dissociation boundary, but above the CSC phase (point B in Fig. 1). In the homogeneous limit, there is one sharp peak at $\omega = 0$. The non-zero width of this peak implies that the diquark is unstable. When temperature grows, the diquarks dissociate, so the peak is replaced by a broad bump shown in the lower panel (corresponding to point D in Fig. 1). In the three panels (from top to bottom) of Fig. 3 we show $\rho_{R,3}$, $\rho_{I,3}$ and $\rho_{i,1/2}$ in the CSC phase (point C in Fig. 1), respectively. For $\rho_{I,3}$ there are δ-function-like peaks in the range $|\omega| < 2\Delta$, indicating stable diquarks. For $\rho_{R,3}$ and $\rho_{i,1/2}$, these peaks attain a small width. Also, as $\mathbf{p}$ increases, all peaks become wider. Note that the spectral densities are not odd functions of ω, because μ_q is non-zero. We see that stable diquarks only exist in the CSC region. Unstable diquark poles outside the CSC re-

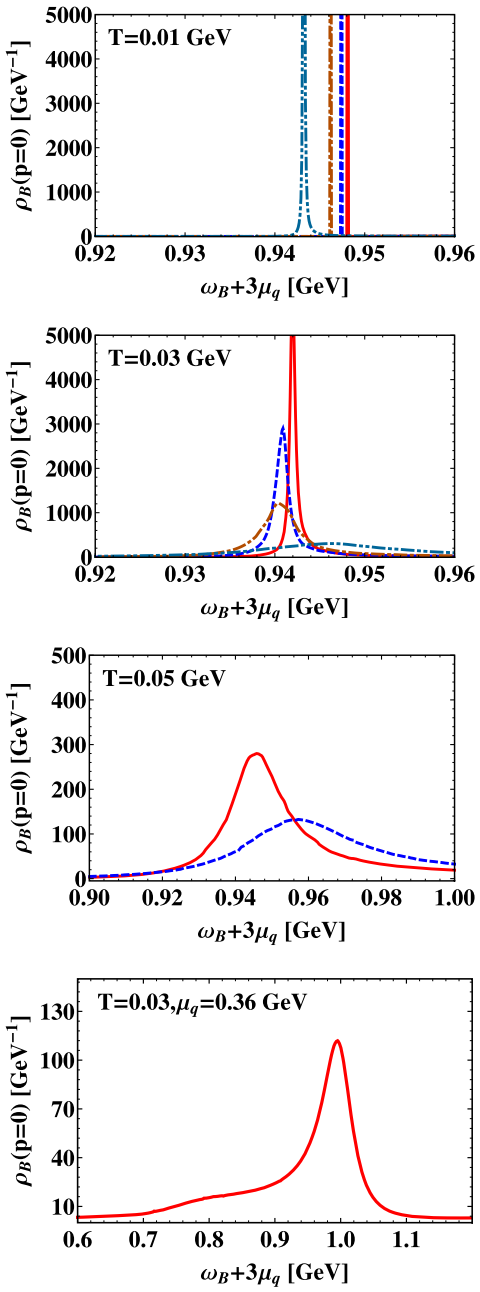

Fig. 5. The baryon spectral densities at different values of T and μ_q as functions of $\omega + 3\mu_q$ for $\mathbf{p} = \mathbf{0}$. Four values of μ_q are chosen for each panel, 0.29 GeV (red solid), 0.30 GeV (blue dashed), 0.31 GeV (brown dash-dotted) and 0.32 GeV (light blue dash-dot-dotted). In the fourth panel (from top to bottom) we show the result for $T = 0.03$ GeV and $\mu_q = 0.36$ GeV (point C of Fig. 1). (For interpretation of the references to color in this figure, the reader is referred to the web version of this Letter.)

gion are actually the diquark fluctuations discussed in Ref. [33]. One can also see from the lower two panels that there are five Nambu–Goldstone (NG) modes which have poles at $\omega = 0$ for zero momenta. In the lowest panel, there are four NG modes, i.e., the real and imaginary scalar fields with red and green color. In the middle panel, there is one NG mode for the imaginary scalar field with blue color. These existence of these NG modes is due to the validity of the following equations: $\frac{1}{2}\Pi_{I/R,1/2}(0,\mathbf{0}) + \frac{1}{4G_D} = 0$ and $\frac{1}{2}\Pi_{I,3}(0,\mathbf{0}) + \frac{1}{4G_D} = 0$.

In Fig. 4 we show the real and imaginary parts of the inverse retarded Greens function for baryons (positive energy component),

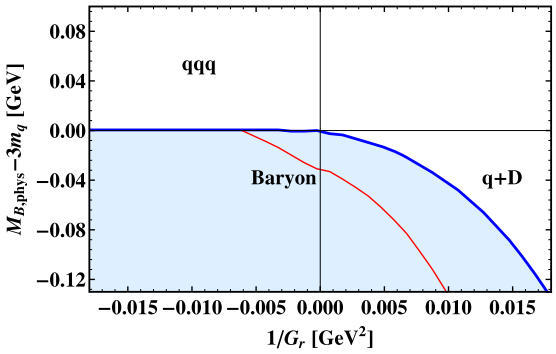

Fig. 6. The quantity $\omega_B + 3(\mu_q - m_q)$ as a function of the inverse renormalized coupling $1/G_r$ at $T = \mu_q = 0$. In the shaded region, i.e., below the blue curve, baryons are stable. The red curve inside this region is given by $M_{B,phys} - 3m_q$, where $M_{B,phys}$ is the physical mass of the baryon. (For interpretation of the references to color in this figure, the reader is referred to the web version of this Letter.)

again at points A, B, C, and D in the phase diagram of Fig. 1. In the phase of broken chiral symmetry with $m_q \neq 0$ and $\Delta = 0$ (point A), there are no diquark condensates or resonances but there are stable baryon resonances: in the first panel (from top to bottom), we see that $\mathrm{Re}\, S_{B+}^{-1}(\omega_B, \mathbf{0}) = 0$ has a solution at $\omega_B + 3\mu_q \approx 0.94$ GeV, i.e., close to the rest mass of the nucleon. There is a region of $\omega_B \in [-3(m_q + \mu_q), 3(m_q - \mu_q)]$ or $M_B \in [-3m_q, 3m_q]$, where the imaginary part $\mathrm{Im}\, S_{B+}^{-1}(\omega_B, \mathbf{0})$ is very small (smaller than 10^{-6} GeV) in the homogeneous limit. The position is just inside this region, i.e., $M_B < 3m_q$: the baryon weighs less than its constituents. It is therefore stable, although its constituents by themselves are unbound, like in a Borromean state in atomic or nuclear physics.

The second panel shows the case with diquark resonances but outside the CSC phase (point B). There is no positive energy baryon pole in this case. In the region of higher temperatures and quark chemical potentials where chiral symmetry is restored and where there are neither diquark condensates nor resonances (point D), there are also no baryon resonances and the absolute value of $\mathrm{Im}\, S_{B+}^{-1}$ is very large. This case is shown in the third panel. In the CSC phase (point C), there are baryon poles but with large imaginary parts, indicating unstable baryon resonances, as shown in the fourth panel. This is confirmed by a broad bump in the baryon spectral density in the fourth panel of Fig. 5.

The results for the baryon spectral density at different values of T and μ_q are presented in Fig. 5. In the first and second panels (from top to bottom), where $T = 0.01, 0.03$ GeV, we observe that the baryon spectral density hardly changes with respect to its width or peak position when varying the chemical potential from 0.29 to 0.32 GeV. In the third panel with $T = 0.05$ GeV the peak position shows a small increase with increasing μ_q. For these larger temperatures, however, the width shows a dramatic increase: the curves for $(T, \mu_q) = (0.05, 0.31), (0.05, 0.32)$ GeV are not even visible on the current scale, implying the disappearance of the baryon resonances. For the curves still visible at $T = 0.05$ GeV, the widths are very large indicating highly unstable baryon resonances. In the CSC phase with $(T, \mu_q) = (0.03, 0.36)$ GeV (the fourth panel) the baryon resonance is also quite unstable, since the peak is very low and broad on the scale of the other panels in this figure.

In Fig. 6 we vary the diquark coupling constant in order to investigate where the baryon is stable at $T = \mu_q = 0$. We choose as x-axis the renormalized coupling G_r defined in Eq. (40) of Ref. [17]. The advantage of using G_r instead of G_D is that the existence of stable diquark bound states is determined by the sign of G_r: for $G_r > 0$ we have diquark bound states, for $G_r < 0$ they do not exist. The shaded region in Fig. 6 indicates where baryons are stable,

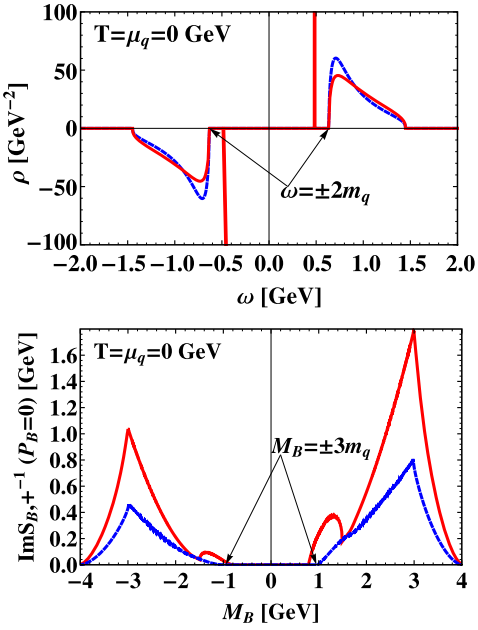

Fig. 7. The diquark spectral density (upper panel) and the imaginary part of the inverse baryon propagator (lower panel). The red solid lines are results for $G_D = 5.95$ GeV^{-2} and the blue dashed lines are for $G_D = 3.11$ GeV^{-2}. (For interpretation of the references to color in this figure, the reader is referred to the web version of this Letter.)

i.e., where the imaginary part of the inverse baryon propagator vanishes, or where the spectral density may exhibit a δ-function-like peak (provided the real part also vanishes inside this region). Above the blue curve the system is in a three-quark state (for weak diquark coupling) or in a quark–diquark state (for strong diquark coupling). At moderately weak negative G_r the diquark is not stable, but, as indicated by the red curve, we obtain a stable baryonic bound state with mass $M_{B,phys} < 3m_q$, where $M_{B,phys}$ is defined as the location of the peak position of the baryon spectral density. If we increase G_r towards positive values, i.e., in the range where diquarks are stable, the pole energy of a stable baryonic bound state must lie in the range $[-(\omega_D + 2\mu_q) - m_q, \omega_D + 2\mu_q + m_q]$ (ω_D is the energy of the diquark at $\mathbf{p} = \mathbf{0}$). The upper boundary of this range corresponds to the blue curve which is consequently given by $\omega_D + 2\mu_q - 2m_q$.

The threshold for stable baryons shown in Fig. 6 by the blue curve is similar to the boundary for Efimov states in non-relativistic cold atom physics: there, the boundary is proportional to $-1/a_s^2$, where a_s is the scattering length. In our case, $G_r \sim a_s$, cf. Eq. (39) of Ref. [17]. The curvature of the boundary in Fig. 6 indeed indicates a quadratic behavior as a function of G_r.

The red curve for the baryon bound state was computed with a fixed coupling constant G_B. There are some similarities between this state and an Efimov state. Also there, the latter cannot form, if the two-body coupling constant is too weak, i.e., for small negative G_r. On the other hand, for a very strong two-body coupling, i.e., for small positive G_r, there may be a competition between the two-body bound state and the three-body bound state. There are also differences to an Efimov state, for instance, in Fig. 6 the baryon bound state does not cross the decay threshold for positive G_r. We perceive this to be an artifact of a fixed quark–diquark coupling G_B in our model. In a full calculation the quark–diquark coupling G_B should vary proportional to the inverse (dressed) mass of the quark exchanged between quark and diquark [26]. Then, G_B will also become a function of the diquark coupling constant G_D. A characteristics of Efimov physics is an infinite tower of higher-lying excited states. In order to show that they also occur in our case, we would have to solve an eigenvalue equation for baryonic bound states. This is a subject for future investigations.

In order to see the interplay between the stable diquark and baryon more explicitly, we present in Fig. 7 the diquark spectral density and the imaginary part of the inverse baryon propagator for $T = \mu_q = 0$ GeV. For a strong diquark coupling (red solid line), one finds two components in the spectral density, a continuous component ρ_c and a pole one,

$$\rho_\delta(\omega, \mathbf{p}) = A(p)\delta\big[\omega - \omega_p(p)\big] - A(p)\delta\big[\omega + \omega_p(p)\big], \tag{11}$$

where the amplitude is given by $A(p) = (\partial\,\mathrm{Re}\,\Pi/\partial\omega)^{-1}|_{\omega=\omega_p(p)}$, and $\omega_p(p)$ is the energy of the pole with $p = |\mathbf{p}|$. If the diquark coupling is weak (blue dashed line), only the continuous component remains, indicating an unstable diquark. Both components are taken into account in calculating the baryon self-energy. From the imaginary part of the inverse baryon propagator, one finds a region $M_B \in [-3m_q, 3m_q]$ where $\mathrm{Im}\,S^{-1}_{B,+} = 0$ GeV in the weak-coupling case $G_D = 3.11$ GeV^{-2} (blue dashed line), where a stable baryon can be formed. In the strong-coupling case $G_D = 5.95$ GeV^{-2} (red solid line), two additional bumps appear which overlap with the window $M_B \in [-3m_q, 3m_q]$. Since non-zero $\mathrm{Im}\,S^{-1}_{B,+}$ indicates unstable baryons, the region for stable baryons is reduced. This shows that the interplay between pole and continuum part of the diquark spectral density is an important ingredient in the formation of baryons. Neglecting the latter and taking only the pole part into account misses important physics (such as the formation of a Borromean-type stable baryon from an unstable diquark and a quark).

Finally, we would like to make some comparison to previous works. In the Faddeev approach [22,23], it is assumed that the baryon is stable and the baryonic T-matrix has a separable form, which reduces the full Faddeev equation to the Bethe–Salpeter equation (BSE) for the baryonic vertex. Furthermore, for numerical simplicity it is also assumed that the diquark is stable. Thus, the baryon mass can be obtained via solving an eigen-equation (i.e., BSE) for the baryonic vertex. In this approach, the effect of temperature was so far neglected due to the increase in numerical complexity. An unstable diquark would also make the equation numerically hard to solve. Thus, so far the baryon was only treated as a stable bound state of a quark and a stable diquark. Since the baryon is stable by assumption, the properties of baryon resonances cannot be obtained in the Faddeev approach, where the baryon dissociation condition is simply realized by the condition that the baryon mass exceeds the sum of quark and diquark masses. However, this baryon dissociation condition is not correct in the CSC region where quarks are gapped. The correct way is to find if there are δ-function-like peaks in the baryon spectral density, as done in this Letter. Our static approximation simplifies the Faddeev equation to an RPA-type quasi-fermion BSE, so the baryon formation and dissociation at non-zero temperature and chemical potential is amenable to treatment. As we have shown, we have calculated the full baryonic spectral densities in different phases, from which the baryon dissociation condition is correctly obtained.

The authors of Refs. [24,25] also used the static approximation in order to simplify the Faddeev equation, but they focus on different issues. For the diquark propagator, they used the proper-time regularization method which introduces an effective confinement, but the method is not applicable to non-zero temperature. The diquark T-matrix is approximated by a constant term $1/4G_D$ plus pole terms, which is equivalent to taking a stable diquark, while we employ the full spectral density of the diquark. There is some difference between our results and theirs. At low temperatures we also calculated the baryon mass as a function of chemical po-

tential: we find only a slight decrease of the baryon mass with chemical potential, while they obtain a significant decrease. The reason is that we did not include vector mesons and thus do not obtain large baryon number densities. Also we did not find a way of introducing confinement at non-zero temperature. We plan to look at these issues in a future study. In Ref. [26], the static approximation and a stable diquark are used. The authors considered a three-flavor NJL model, and the baryon mass is found to decrease by 25% at normal nuclear matter density. We also plan to extend our model to the three-flavor case and study the properties of nuclear matter in the future.

In conclusion, we used an NJL-type model to compute the full diquark propagator and its spectral density in different regions of the phase diagram of strongly interacting matter. Baryon formation and dissociation in dense nuclear and quark matter is then studied via the baryon poles and spectral densities, incorporating the previously obtained diquark propagator. We find that stable baryon resonances with zero width are present in the phase of broken chiral symmetry. There are no baryon poles in the chirally symmetric phase. In the CSC phase, baryon poles exist, but they are found to be unstable due to a sizable width. We also pointed out that the stable baryon states found by us have some similarities to Borromean and Efimov states in atomic or nuclear physics.

Acknowledgements

J.C.W. and Q.W. thank Jian Deng for many insightful discussions especially in the technique of principal value integration, and thank Lian-yi He for helpful discussions. Q.W. is supported in part by the '100 talents' project of Chinese Academy of Sciences (CAS) and by the National Natural Science Foundation of China (NSFC) under Grant Nos. 10675109 and 10735040. J.C.W. is supported in part by China Scholarship Council.

References

[1] M. Gell-Mann, Phys. Lett. 8 (1964) 214.
[2] M. Ida, R. Kobayashi, Prog. Theor. Phys. 36 (1966) 846.
[3] D.B. Lichtenberg, L.J. Tassie, Phys. Rev. 155 (1967) 1601.
[4] G.V. Efimov, M.A. Ivanov, V.E. Lyubovitskij, Z. Phys. C 47 (1990) 583.
[5] M. Anselmino, E. Predazzi, S. Ekelin, S. Fredriksson, D.B. Lichtenberg, Rev. Mod. Phys. 65 (1993) 1199.
[6] A. Buck, R. Alkofer, H. Reinhardt, Phys. Lett. B 286 (1992) 29.
[7] N. Ishii, W. Bentz, K. Yazaki, Phys. Lett. B 318 (1993) 26.
[8] L.J. Abu-Raddad, A. Hosaka, D. Ebert, H. Toki, Phys. Rev. C 66 (2002) 025206, arXiv:nucl-th/0206002.
[9] B.S. Zou, D.O. Riska, Phys. Rev. Lett. 95 (2005) 072001, arXiv:hep-ph/0502225.
[10] M.G. Alford, K. Rajagopal, F. Wilczek, Phys. Lett. B 422 (1998) 247, arXiv:hep-ph/9711395.
[11] R. Rapp, T. Schafer, E.V. Shuryak, M. Velkovsky, Phys. Rev. Lett. 81 (1998) 53, arXiv:hep-ph/9711396.
[12] R.D. Pisarski, D.H. Rischke, Phys. Rev. D 61 (2000) 051501, arXiv:nucl-th/9907041.
[13] D.K. Hong, V.A. Miransky, I.A. Shovkovy, L.C.R. Wijewardhana, Phys. Rev. D 61 (2000) 056001, arXiv:hep-ph/9906478;
D.K. Hong, V.A. Miransky, I.A. Shovkovy, L.C.R. Wijewardhana, Phys. Rev. D 62 (2000) 059903 (Erratum).
[14] M.G. Alford, A. Schmitt, K. Rajagopal, T. Schafer, Rev. Mod. Phys. 80 (2008) 1455, arXiv:0709.4635 [hep-ph].
[15] Q. Wang, Prog. Phys. 30 (2010) 173, arXiv:0912.2485 [nucl-th].
[16] H. Abuki, T. Hatsuda, K. Itakura, Phys. Rev. D 65 (2002) 074014, arXiv:hep-ph/0109013.
[17] H. Abuki, Nucl. Phys. A 791 (2007) 117, arXiv:hep-ph/0605081.
[18] M. Kitazawa, D.H. Rischke, I.A. Shovkovy, Phys. Lett. B 663 (2008) 228, arXiv:0709.2235 [hep-ph].
[19] P. Senger, T. Galatyuk, A. Kiseleva, D. Kresan, A. Lebedev, S. Lebedev, A. Lymanets, J. Phys. G 36 (2009) 064037.
[20] T. Hatsuda, T. Kunihiro, Phys. Rept. 247 (1994) 221, arXiv:hep-ph/9401310.
[21] M. Buballa, Phys. Rept. 407 (2005) 205, arXiv:hep-ph/0402234.
[22] N. Ishii, W. Bentz, K. Yazaki, Nucl. Phys. A 587 (1995) 617.
[23] S. Pepin, M.C. Birse, J.A. McGovern, N.R. Walet, Phys. Rev. C 61 (2000) 055209, arXiv:hep-ph/9912475.
[24] W. Bentz, A.W. Thomas, Nucl. Phys. A 696 (2001) 138, arXiv:nucl-th/0105022.
[25] W. Bentz, T. Horikawa, N. Ishii, A.W. Thomas, Nucl. Phys. A 720 (2003) 95, arXiv:nucl-th/0210067.
[26] F. Gastineau, J. Aichelin, AIP Conf. Proc. 739 (2005) 398.
[27] Y. Nishida, H. Abuki, Phys. Rev. D 72 (2005) 096004, arXiv:hep-ph/0504083.
[28] J. Deng, A. Schmitt, Q. Wang, Phys. Rev. D 76 (2007) 034013, arXiv:nucl-th/0611097.
[29] G.f. Sun, L. He, P. Zhuang, Phys. Rev. D 75 (2007) 096004, arXiv:hep-ph/0703159.
[30] T. Brauner, Phys. Rev. D 77 (2008) 096006, arXiv:0803.2422 [hep-ph].
[31] H. Abuki, G. Baym, T. Hatsuda, N. Yamamoto, Phys. Rev. D 81 (2010) 125010.
[32] H. Basler, M. Buballa, Phys. Rev. D 82 (2010) 094004, arXiv:1007.5198 [hep-ph].
[33] M. Kitazawa, T. Koide, T. Kunihiro, Y. Nemoto, Prog. Theor. Phys. 114 (2005) 117, arXiv:hep-ph/0502035.